Journal of King Saud University – Science 32 (2020) 3103–3110

Contents lists available at ScienceDirect

Journal of King Saud University – Science

journal homepage: www.sciencedirect.com

Original article

Synthesis and photocatalytic performance of Ag-TiVOX nanocomposite

Mahubedu Khutso Ntobeng, Patrick Ehi Imoisili, Ten-Chien Jen *

University of Johannesburg, Johannesburg, Kingsway and University Road, Auckland Park, 2092, P. O. Box 524, Auckland Park, 2006, Johannesburg, South Africa

ARTICLE INFO

Article history:
Received 18 June 2020
Revised 26 August 2020
Accepted 27 August 2020
Available online 4 September 2020

Keywords:
Titanium
Nanocomposite
Methylene blue
Photocatalyst
Band gap

ABSTRACT

A silver, vanadium and silver/vanadium doped titanium dioxide (TiO2, Ag-TiO2, V-TiO2 and Ag-TiVOX) nanocomposite photocatalyst was achieved via a modify sol–gel and hydrothermal method. Structural analysis by X-Ray Diffraction (XRD) depicted the lattice fringes for both anatase and rutile in its crystalline phase in the synthesized nanocomposites. Surface areas (SBET) analysis shows that surface area of synthesized Ag-TiVOX is 46.01 m2/g, compare to TiO2 64.75 m2/g, Ag-TiO2 61.33 m2/g and V-TiO2 62.73 m2/g. Optical absorption results demonstrated by UV–Visible Spectroscopy (UV–Vis) shows that the effects of Ag and V doping was a shift in spectrum to the visible light region, enhancing the visible light absorption capacity of the synthesized photocatalyst. The optical absorption of Ag-TiVOX achieved a reduced bandgap energy of 2.2 eV, as compared to Ag-TiO2 (2.8 eV), V-TiO2 (2.3 eV) and TiO2 (2.9 eV). Morphological characterization by Transition Electron Microscope (TEM) and Scanning Electron Microscope (SEM), depicting a cluster composed of spherical aggregates particles of non-uniform diameter nanoparticles with particle size ranging between 10 and 50 nm. Synthesized Ag-TiVOx demonstrated remarkable photocatalytic capabilities under visible light irradiation, as 99.83 percent of methylene blue (MB) degradation was accomplished during the first 15 min. Impact of Ag and V doping of TiO2 showed enhancement in the photocatalytic activity, reporting excellent removal rates and achieving well desirable decline in the band gap energy.

1. Introduction

A photocatalyst is a substance that helps speed up and improve a light-induced reaction deprived of consumption in the process. The important of photocatalyst activities include water remediation, enhance the quality of atmospheric air, chemical clean-up of oil spills and other contaminants (Pawar et al., 2018). The utilizations of TiO_2 as a photocatalyst has gain prominence as an upshot of its photocorrosion resistance, low cost, biological and chemical stability (Li et al., 2020; Bourezgui et al., 2020). Nevertheless TiO_2 has three major drawbacks, these are higher bandgap value (3.2 eV), photocatalytic UV active only, quick recombination speed of photo-generated electron hole pair and in aqueous solutions, small quantum yield of photocatalytic reactions (Schneider et al., 2014; Gázquez et al., 2014; Díaz-Uribe et al., 2018).

Researchers has suggested that, synthesis method and surface alteration by metal transfer deposition (e.g. platinum, ruthenium, palladium, and silver) as two major strategies to resolve this drawback (Rahimi et al., 2016; Bumajdad and Madkour, 2014; Choi et al., 2010). However, in improving TiO_2 photocatalytic performance, dopant additions is the most effective procedures adopted (Shi et al., 2019; Zhu et al., 2018; Hwang et al., 2011). This can lengthen the array of excitable radiation into the visible region and also alter the grain and surface morphologies (Chen et al., 2017), this results in better visible light absorption and an improvement in the amount of surface-active sites accessible for reactions (Sanzone et al., 2018; Bouzid et al., 2015). Doped TiO_2 based photocatalyst have been considered the superlative candidates in solar powered water purification schemes and often used as a low-cost source of alternate Industry requirements for transparent conductive oxides, such as In_2O_3:Sn (ITO) (Ruffino et al., 2011; Sangpour et al., 2010). Some of the most frequently used and effective dopants of TiO_2 is Ag (Shi et al., 2019; Ismail, 2012; Faisal et al., 2016). Doping TiO_2 with Ag will efficiently increase the degradation performance of photo-catalytic reactions. They function as an electron traps that facilitates interfacial load transmission processes in composite network as a consequence, further photo-induced holes would have the ability to engage in surface

* Corresponding author.
E-mail address: tjen@uj.ac.za (T.-C. Jen).
Peer review under responsibility of King Saud University.

Production and hosting by Elsevier

https://doi.org/10.1016/j.jksus.2020.08.021
1018-3647/

oxidation reactions (Weng and Han, 2017; Ismail and Matsunaga, 2007). Among metal ions, the ionic radius of vanadium is virtually equal to that of titanium, and can easily be doped into TiO_2. Vanadium-doped TiO_2 at low concentrations have been identified to boost the photocatalytic ability of TiO_2, contributing to an increase in the existence of the photo-generated charge and extended absorption range more effectively than other metal ions (Shao et al., 2015; Yang et al., 2010; Tripathi et al., 2010).

From previous work, Tripathi et al. (2010), developed silver, vanadium sensitized titanium mixed metal oxides using titanium isopropoxide ($C_{12}H_{28}O_4Ti$) as precursor to TiO_2, vanadium pentoxide (V_2O_5) as precursor to vanadium and silver chloride (AgCl) as precursor to silver chloride (AgCl). While Zhu et al. (2018) uses tetrabutyl orthotitanate ($C_{16}H_{40}O_4Ti$), as titanium precursor, triisopropoxyvandium (V) oxide ($C_9H_{21}O_4V$) as vanadium precursor and silver nitrate ($AgNO_3$) as silver sources in the synthesis of a ternary nanostructure $Ag/V_2O_5/TiO_2$ for methyl orange degradation. Both study report an improve photocatalytic performance of Ag-TiO_2 with Vanadium doping. For this investigation, titanium (IV) butoxide [$Ti(OCH_2CH_2CH_2CH_3)_4$] was used as a precursor to titanium, ammonium metavanadate (NH_4VO_3) as a precursor to vanadium and silver nitrate ($AgNO_3$) as a silver precursor, to synthesise a silver and vanadium mixed oxides titanium (Ag-$TiVO_x$) nanostructured composite, using a modified sol–gel and hydrothermal method . This is a combination of two simple methods for synthesis of nanomaterial at low temperature. The employment of a modified sol–gel and hydrothermal technique aid the preparation of a highly effective visible light driven doped Ag–$TiVO_x$ semiconductive photocatalyst composite. The microstructural, optical, chemical, and photocatalytic charateristic of the nanostructured composite was assessed. In order to evaluate the photocatalytic performance of Ag-$TiVO_x$, as compare with TiO_2, Ag-TiO_2 and V-TiO_2 nanocomposite, MB photo-degradation under visible light irradiation was investigated.

2. Material and methods

2.1. Materials synthesis

Chemicals used in this experimental, were analytical grade and supplied by Merck. TiO_2 based photocatalyst TiO_2, Ag-TiO_2, V-TiO_2 and Ag-$TiVO_x$ composite, was fabricated by a sol–gel and hydrothermal method. To prepare TiO_2, 1 ml of Titanium (IV) butoxide was hydrolysed with 50 ml of deionised water (DI). The solution was then decanted after 10 mins. Thereafter 5 ml of hydrogen peroxide was added to the mixture along with 25 ml of deionised water, allowed for the formation of a gel like mixture. The gel was autoclaved in a stainless Teflon steel flask at 180 °C for 4 h. Followed by cooling at room temperature. It was then centrifuged and washed multiple times with ethanol and DI. The resulted precipitant was then kept in the oven at 80 °C to dry for 12 h. To synthesize Ag-TiO_2, 1 ml of Titanium (IV) butoxide was hydrolysed with 50 ml of DI. The solution was then decanted after 10mins and, 5 ml of hydrogen peroxide was added along with along with 5 ml of $AgNO_3$ (10 mg/l) and 25 ml of DI water. Continuous stirring was applied to the solution, until the formation of a gel, and then the solution was autoclaved at 180 °C for 4 h. The samples was centrifuged after cooing, and washed multiple times with ethanol and DI water. The resulted precipitant was oven dried at 80 °C for 12 h. For V-TiO_2 synthesis, the procedure above was repeated with 0.1 g of NH_4VO_3 instead of $AgNO_3$. While for Ag-$TiVO_x$ photocatalyst composite synthesis, 5 ml of both $AgNO_3$ and NH_4VO_3 was added to the TiO_2 mixture to fabricate Ag-$TiVO_x$ nanocomposite

2.2. Characterization

The crystal structure and phase purities were analysed, by (XRD) Diffractometer (X-Pert Philips), from 2θ 10° to 90° at 40 kV voltage and 40 μA current. The Brunauer-Emmett-Teller (BET) was utilized in analysing the surface area of the nanocomposite material, using micrometrics ASAP 2460. The ultraviolet visible diffuse reflection spectroscopy (UV–vis DRS) were recorded using Cary 5000, UV–Vis-NIR spectra-photo meter with a DRA inserter. The surface morphology were analysis using a SEM (ZEISS-AurigaCobra SEM, Oberkochen, Germany) and a TEM (JEM-2100 JEOL), connected with EDS CCD camera.

2.3. MB photo-degradation test

Photocatalytic activity test was conducted by analysing the changes in dye concentration after concentration reactions under visible light illumination utilising MB as a control pollutant in a photocatalytic reactor. MB ($C_{16}H_{18}ClN_3S$), is a heterocyclic aromatic chemical substance which has numerous usages in series of disciplines, such the chemical sciences (biology and chemistry). This occurs as an odourless, dark-green solid, material that produces a bluish solution when soluble in H_2O at room temperature. The colour is long-lasting and incompatible with reducing agents, heavy oxidizing agents and bases. In a biological or chemical reaction, cycle such dye compounds not just diminish dissolved oxygen in water sources, but also emit other hazardous compounds that endanger marine life (Dolgonos et al., 2016). In the experiment 10 mg/l of the MB solution was prepared and used as model pollutant. 0.1 g of the photocatalyst was dissolved in 50 ml of MB solution, were then irradiated with a lamp ($\lambda \geq 254$ nm, eight 9 W compact Fluorescent Integrated lamp 220–240 V, 50–60 Hz mini white E14 cool daylight lamps Philips, Holland), as a visible source of illumination. The solution was mechanically stirred, while exposure to visible light illumination. Aliquots of 1.5 ml was collected from the solution and filtered through 0.2 μm PTFE syringes, at intervals of 15 mins for 1 h. The degradation efficacy for MB was calculated using Eq. (1)

$$Eff(\%)\left[C_o - \frac{C}{C_o}\right] \times 100 \quad (1)$$

Were, C_O is the initial absorption of MB preceding the photocatalytic operational testing. C is the MB final concentration after photocatalytic degradation (mg/L) at the appropriate time interval (Dolgonos et al., 2016).

3. Result and discussion

3.1. XRD analysis

Fig. 1(a) illustrates the phase diffraction peaks for TiO_2, Ag-TiO_2, V-TiO_2, Ag-$TiVO_x$. The diffraction peaks illustrate the combine crystallinity phases of anatase and rutile. The peak for anatase appears at a 2θ value of 25.3°. The correspondence is with agreement to crystal plane (101) consistent with JCPDS database # 89–4921. Ag-TiO_2 and co-doped Ag, V-TiO_2 exhibit higher anatase phase. It was observed, that the most intense peak for rutile phase appears at 2θ of 27. 4°. The 2θ values for 25.3 and 27.4°, appears in all the XRD patterns for each catalyst, which correspond to crystal planes (101) for anatase and (110) for rutile, respectively (Liu et al., 2019). The cubic phase for Ag-$TiVO_x$ for anatase and rutile are with agreement with JCPDS database (#00-006-9240) and (#00-072-4812). Addition of the dopant causes an increase in the anatase phase, this agrees with results from other studies (Sanzone et al., 2018; Ruffino et al., 2011; Liu et al., 2019).

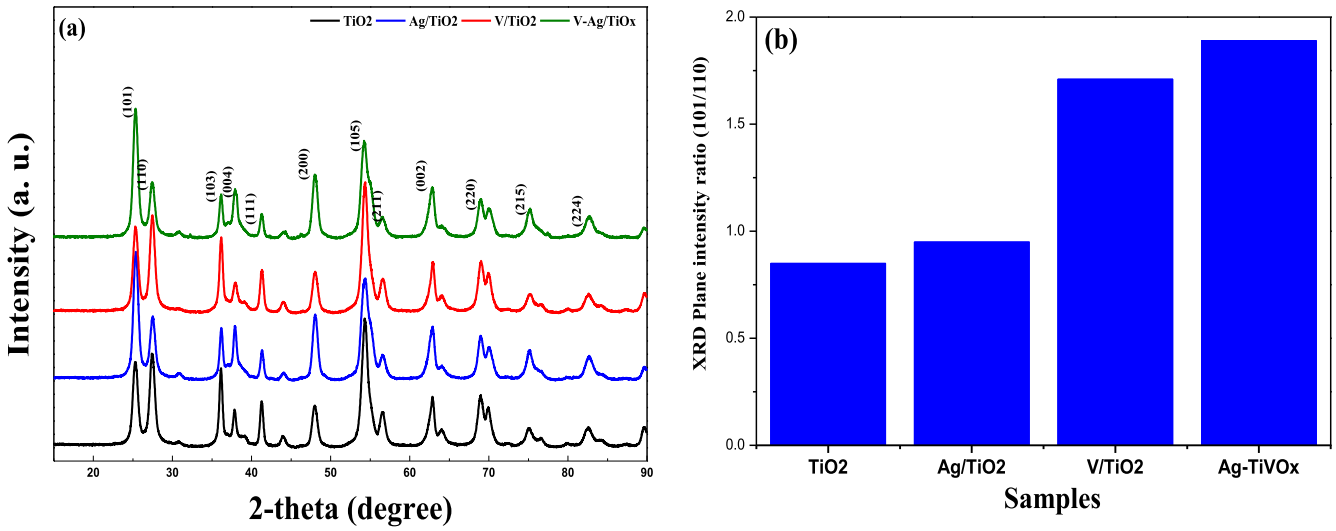

Fig. 1. XRD (a) patterns, (b) Intensity ratios of TiO_2, Ag-TiO_2, V-TiO_2, Ag-$TiVO_x$ samples.

Fig. 1(b), exhibits the change in the (101)/(110) plane intensity ratio for each catalyst. The plane intensity ratio for each catalyst upsurges as the structure of the photocatalyst changes due to doping, with Ag and V with Ag-$TiVO_x$ shows the utmost plane intensity ratio (Liu et al., 2019). The crystalline size was determined using Scherrer rule (0.9 λ/β cos θ) of the line width (FWHM, β) of the most symmetrical then severe height (Imoisili et al., 2018). As shown in Table 1, Ag-$TiVO_x$ oxide scale was estimated to be ≥ 18 nm, this was similar to 20 nm obtain by Tripathi et al., (2010).

3.2. Surface area (S_{BET}) analysis

The Specific Surface Area (S_{BET}) was record and tabulated in Table 2, while the Nitrogen adsorption–desorption isotherm are shown in Fig. 2(a–d). The specific areas record by S_{BET} for TiO_2, Ag-TiO_2, V-TiO_2 and Ag-$TiVO_x$, was 64.75 m^2/g, 61.33 m^2/g, 62.73 m^2/g, and 46.01 m^2/g. As seen, Ag-$TiVO_x$ photocatalyst has the highest surface area owing to their smaller crystallite size. It was explained, that higher specific surface area improves the activity of photocatalyst as it provided more site for light absorption (Liu et al., 2019; Dolgonos et al., 2016; Ren et al., 2009; Reddy et al., 1998).

3.3. UV –Visible spectroscopy (UV–Vis)

Fig. 3(a), demonstrate the absorbance spectrum of each synthesized photocatalyst The absorption edges for TiO_2, Ag-TiO_2 and V-TiO_2 occurs at wavelengths of 405, 404, 473 nm, while Ag-$TiVO_x$ absorption edge shifted to higher wavelength with two additional peak around 550 nm and shoulder around 700 nm. This suggest that the Ag-$TiVO_x$ photocatalyst successfully utilize the visible light spectrum (Liu et al., 2019). Band-gap transitions are indicative in the absorption edges. The effects of co-doing using Ag and V greatly enhances the absorption of light at longer wavelengths (>400 nm) and is the visible light regions. The co-doping with Ag and V indicates significant enhancements in the photocatalytic activity at visible light irradiation. With emphasis on synergistic effects of Ag and V, their effect has led to higher reaction kinetic due to shifting the light absorption to the visible light region therefore harvesting higher amount of energy.

The bang gap energy (eV) calculation was used to evaluate the energy required to activate the photocatalyst. The energy band gap (eV) of each photocatalyst was calcluate by the Tauc equation, as shown in equation 1 (Reddy et al., 1998). where h is Planck constant, ν is photon's frequency, and B is a constant. The γ factor is equal to 1/2 or 2 for the indirect and direct transition band gaps, respectively and depends on the nature of the electron transition

$$(\alpha h\upsilon)^{1/\gamma} = B(h\upsilon - Eg) \quad (2)$$

As shown in Fig. 3(b), the bands gap energies for TiO_2, Ag-TiO_2, V-TiO_2 and Ag-$TiVO_x$ samples were interpolated to be 2.9, 2.8, 2.3, 2.2 (eV) respectively. The doped TiO_2 photocatalyst is seen to have achieve a desirable smaller band energy value which is consistence with previous reported (Liu, et al., 2019; Weng and Han, 2017; Dolgonos et al., 2016). This smaller band gap enables the photocatalyst to be triggered with lesser energy in the visible light region.

3.4. SEM analysis

Ag-$TiVO_x$ been the most reactive photocatalyst as shown in Fig. 4(a), was used as representative sample for SEM surface morphology. As revealed in the SEM, image shows the formation of a regular cluster composed of spherical aggregates particles of non-uniform diameter. The EDX findings as exhibited in Fig. 4(b), of the representative sample (Ag-$TiVO_x$) photocatalyst indicated the existence of Ti, V, Ag, and O elements and the tests were compatible with the XPS findings.

Table 1
Average crystalline size (^{d}XRD) of TiO_2, V-TiO_2, Ag-TiO_2 and Ag-$TiVO_x$ samples.

Photocatalyst	Average crystalline size (nm)
TiO_2	26.56
Ag-TiO_2	24.87
V-TiO_2	24.58
Ag, $TiVO_x$	18.34

Table 2
S_{BET} of synthesized photocatalyst.

Sample	Surface area (m^2/g)
TiO_2	64.75
Ag-TiO_2	61.33
V-TiO_2	62.73
Ag-$TiVO_x$	46.01

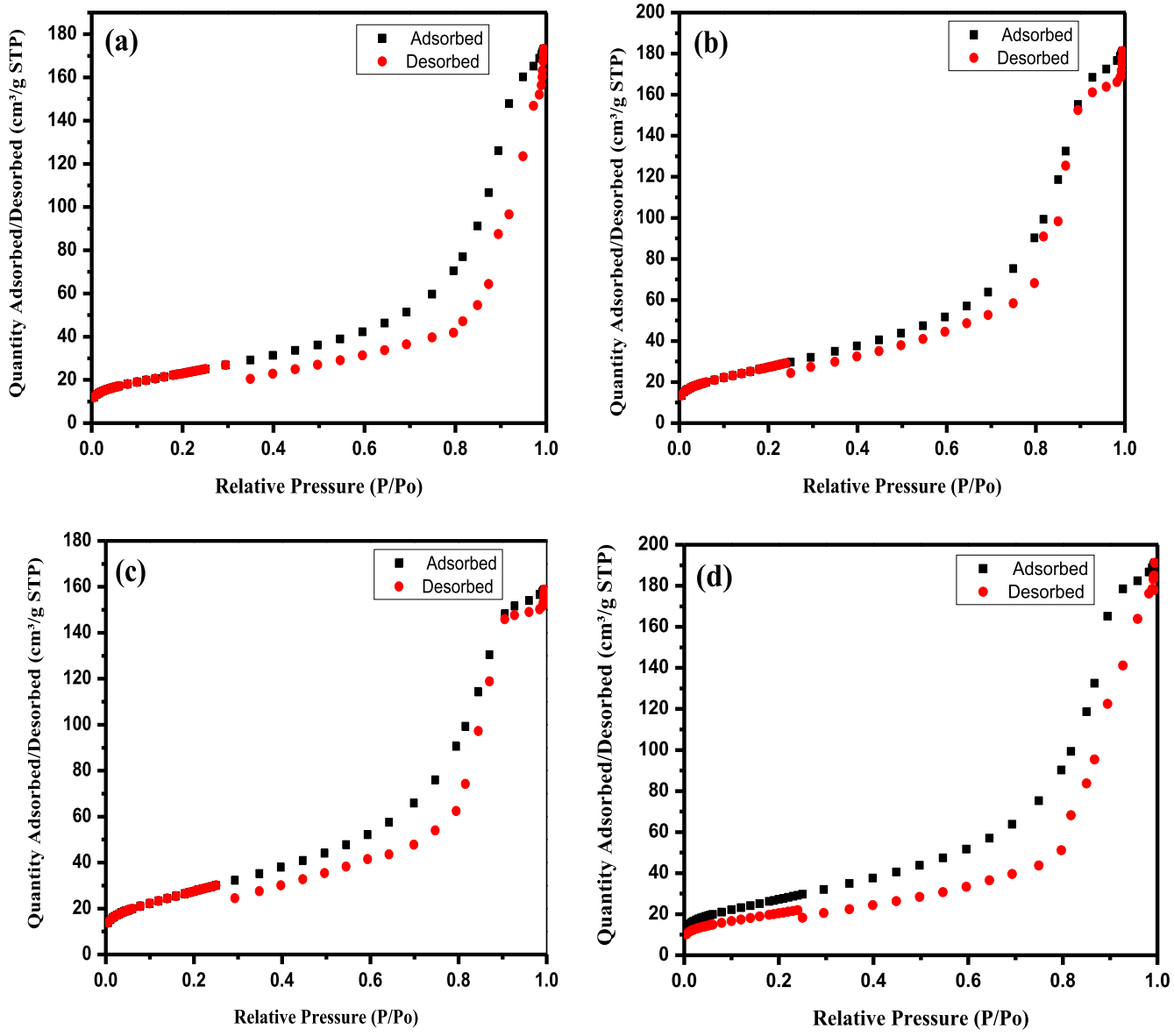

Fig. 2. Nitrogen adsorption–desorption isotherm of (a) TiO_2, (b) V-TiO_2, (c) Ag-TiO_2 and (d) Ag-$TiVO_x$.

3.5. Transmissions electron microscopy (TEM)

HRTEM images and bright field patterns was record and shown in Fig. 5. The synthesis particles were non-uniform roughly rod-like shaped, with a particle size distribution range between 10 and 50 nm. The selected area electron diffraction (SAED) pattern (Fig. 5(b) inset) supports the polycrystalline existence in the fabricated sample. The HRTEM micrograph (Fig. 5(b) reveals the 0.416 and 0.590 nm distance fringes corresponding to (1 1 0) $TiVO_x$ plane and (1 1 1) Ag plane, respectively (Reddy et al., 1998). The TEM findings of this analysis are compatible with those stated by previous studies (Shi et al., 2019; Liu et al., 2019). Nonetheless, separate synthetic methods, surfactant and precursor to titanium, Vanadium and silver were used in this present study to synthesize the Ag-$TiVO_x$ samples

3.6. X-ray photoelectron spectroscopy (XPS)

The chemical structure and valance state of various species was determined and analysed on the surface region of Ag-$TiVO_x$ by XPS. The full XPS scan survey spectrum is show in Fig. 6. The XPS study, shows the binding energy peaks C 1 s core level peaks at 283.09 eV. While the binding energy peaks for Ti $2p_{3/2}$ and Ti $2p_{1/2}$ occurs at peak values of 458.30 and 464.16 eV, signifying the formation of Ti^{4+} in TiO_2 (Liu et al., 2019, 2011; Zhang et al., 2008; Whang et al., 2009). The peaks values of 469.51 and 513.14 eV corresponds to binding energies for V $2p_{3/2}$ and V $2p_{1/}$, illustrating the occurrence of V, on the catalyst surface in the IV state (Reddy et al., 1998). The chemical state of Ag shows large to low binding energy levels at $3d_{5/2}$ and $3d_{3/2}$ correspond to peaks values of 367.4 eV and 373.4 eV (Zhang et al., 2008; Liu et al., 2011). A significant interaction of the Ag nano-sized particles with TiO_2 and V can be seen to have transferred excited electrons, depleting a significant interaction between the TiO_2 and V particles, resulting in excited electrons transfers on the catalyst surface area. Fig. 6, also indicates a significant signal at 528.03 eV, which agrees to the photo transition of O1s; ultimately, the signal found at 283.09 eV relates to the electronic transformation of C 1 s. This signal is characteristic of the ambient CO_2 absorbed on the clear air (Whang et al., 2009; Liu et al., 2011).

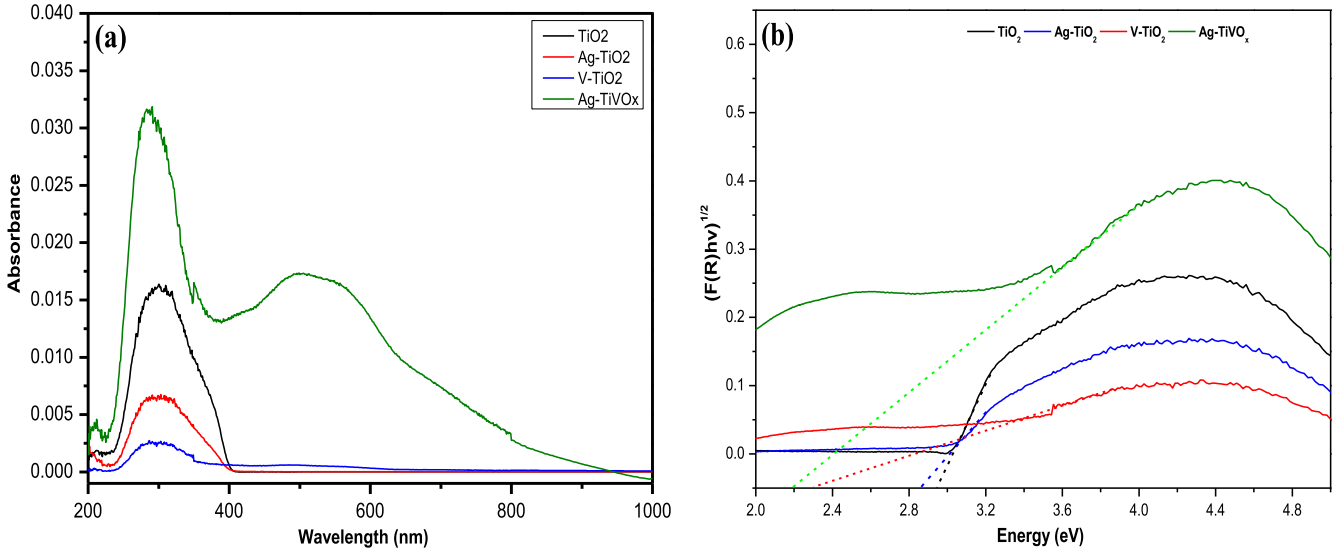

Fig. 3. (a) Absorbance spectrum (b) Energy band gap, of TiO_2, V-TiO_2, Ag-TiO_2 and Ag-$TiVO_x$.

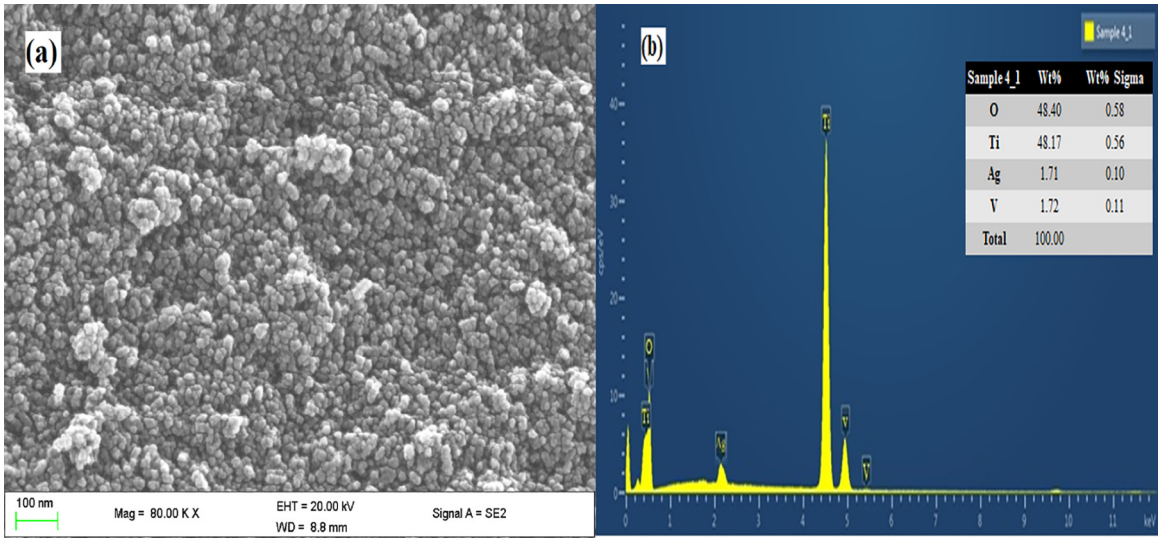

Fig. 4. SEM image (a) Ag-$TiVO_x$ nanocomposite (b) EDX spectral.

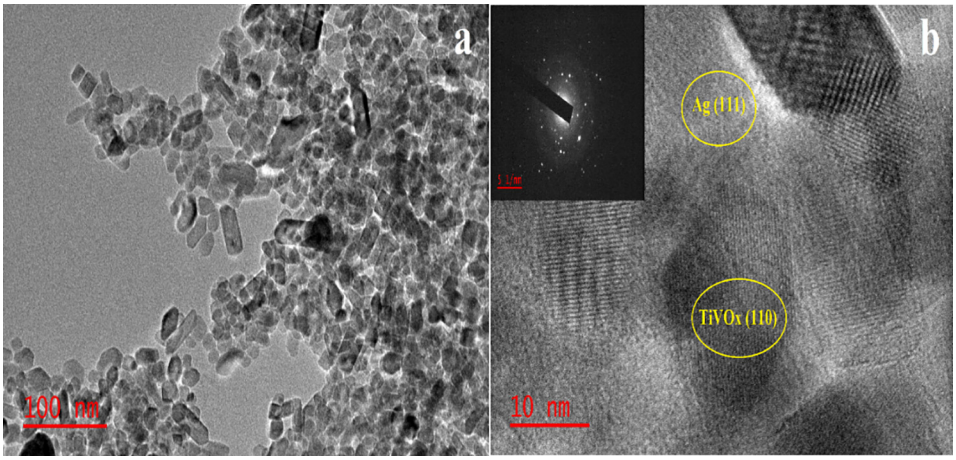

Fig. 5. TEM illustration (a) HRTEM images and SAED template inset (b) of Ag-$TiVO_x$.

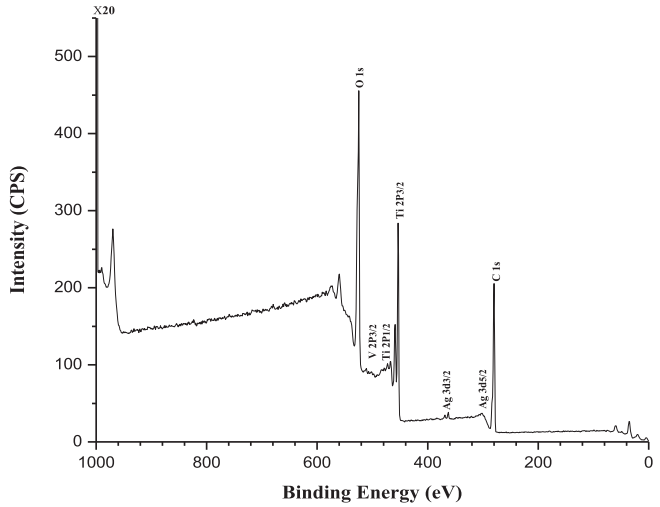

Fig. 6. Full Scan Survey of the Ag-TiVO$_x$ samples.

3.7. Photocatalytic evaluation

3.7.1. Degradation of MB

Photocatalytic evaluation of synthesised photocatalyst was performed by investigating the kinetic degradation of MB solution during visible light irradiation. The MB solutions was exposed to photocatalytic activity beneath visible light by a model reactor for a duration of 60mins with sample extraction at 15 min intervals. The hole and electron are produced in the in the valence band and conduction band of the nanocomposite photocatalyst by UV irradiation, respectively, as shown in (X1) (Wu et al., 2010). The hydroxide ions (or water molecule) are oxidized by the positive hole adsorbed on the surface of Ag-TiVO$_x$ particles to yield hydroxyl radical (Wu et al., 2010), as presented in (X2). For the photosensitized oxidation mechanism, in the existence of the photocatalysts nanocomposite, an electron is inserted into the conducting band by the excited state of MB (X3). The hydroxyl radical present on the photocatalyst nanocomposite surface, fast-tracked the degradation of MB (X5). The transformed of the MB dye to a cationic radical that is degraded to yield products demonstrated by (X4) to (X7) (Le et al., 2012). The variations in absorption reading of the MB solution are presented in Fig. 7. TiO_2 showed poor photocatalytic degradation effect within the first hour under visible light irradiation, with an average removal rate of 73.94% meanwhile the Ag-TiO_2 and V-TiO_2 photocatalyst removed MB with an average removal rate of 82.54% and 82.10%, respectively. In contrast the Ag-TiVO$_x$ photocatalyst exhibited improved activity, with a successful removal rate of 99.33% within 15 min, which is significant in this study.

$$(\mathrm{Ag-TiVOx}) + \mathrm{hv} \rightarrow e^{-}_{CB} + h^{+}_{VB} \quad (1)$$

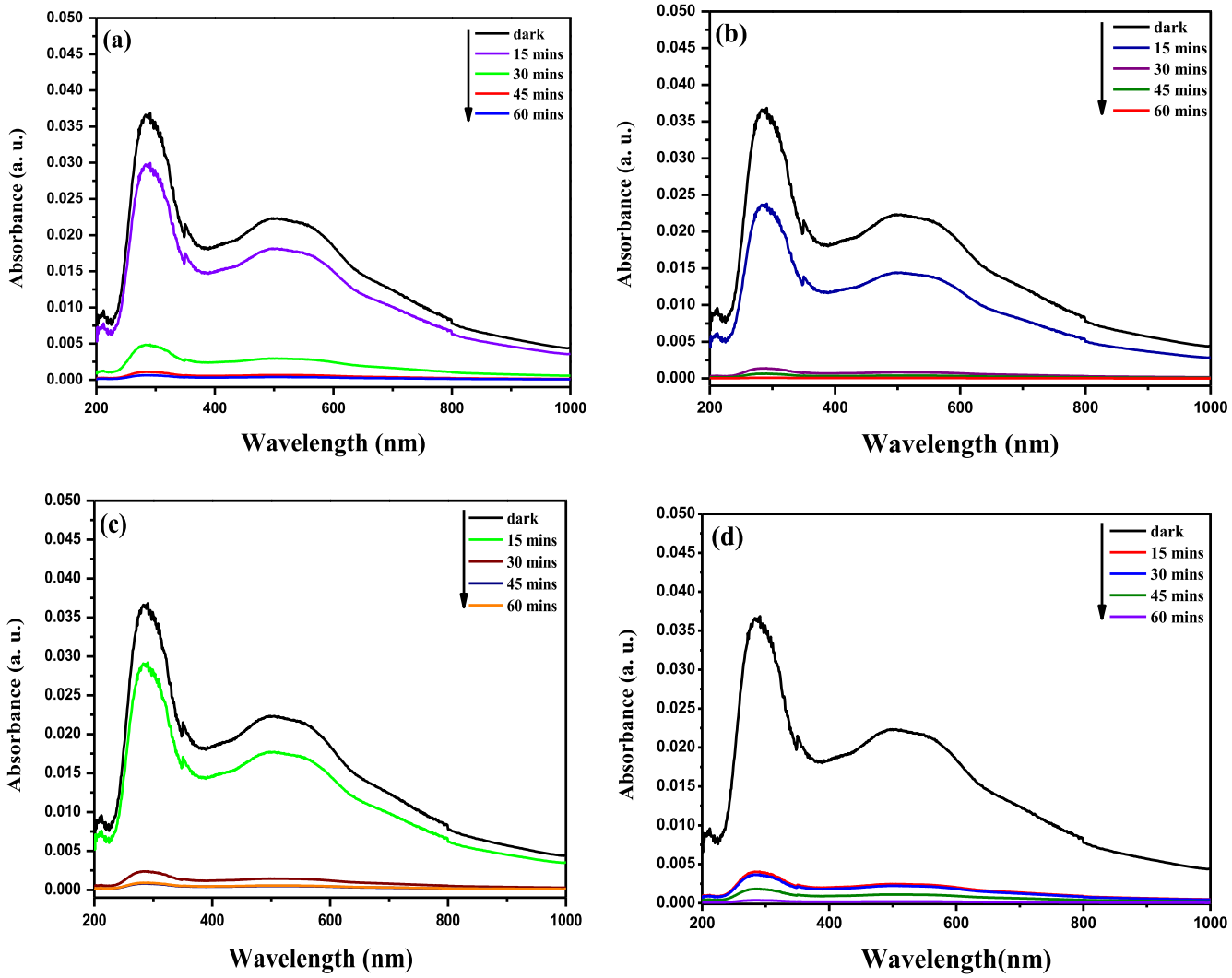

Fig. 7. visible light degradation of MB for (a) TiO_2, (b) Ag-TiO_2, (c) V-TiO_2, and (d) Ag-TiVO$_x$.

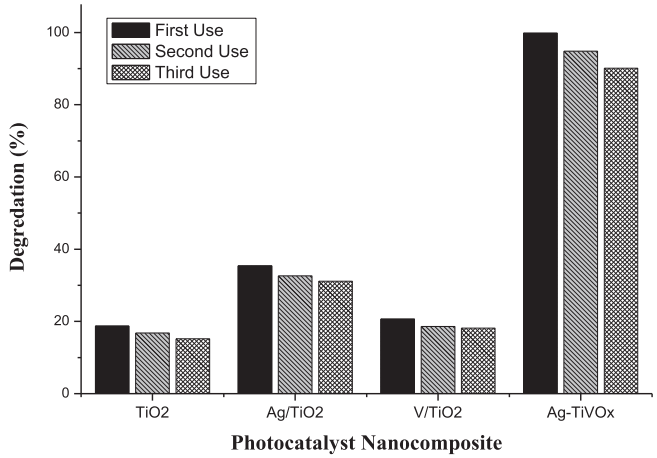

Fig. 8. Usability of synthesized photocatalyst nanocomposite after three utilization.

$$(Ag - TiVOxh_{VB}^{+}) + H_2O \rightarrow Ag - TiVOx + H + OH^{\circ} \quad (2)$$

$$\mathrm{MB} * + \mathrm{TiO_2} \rightarrow \mathrm{MB}^{\circ} + \mathrm{e_{CB}^{-}}(\mathrm{Ag - TiVOx}) \quad (3)$$

$$O_2 + e^{-} \rightarrow O_2^{\circ -} \quad (4)$$

$$\mathrm{MB}^{\circ +} + \mathrm{OH}^{-} \rightarrow \mathrm{MB} + \mathrm{OH}^{\circ} \quad (5)$$

$$MB^{\circ +} + OH^{\circ} \rightarrow products \quad (6)$$

$$\mathrm{MB}^{\circ +} + \mathrm{O_2^{\circ -}} \rightarrow \mathrm{products} \quad (7)$$

The Ag-$TiVO_x$ catalyst has a fairly high rate of MB degradation relative to TiO_2, Ag-TiO_2, and V-TiO_2. Synthesised Ag-$TiVO_x$, photocatalyst achieves 99.83% degradation within the first 15 min. This is a remarkable observation for the activity test indicating that a high active photocatalyst has been synthesised. The findings revealed that the photocatalytic function of titanium dioxideTiO_2 has been significantly enhanced, with the existence of transition metal ions and Ag-$TiVO_x$ was the utmost photocatalyst (Liu et al., 2019, 2011; Whang et al., 2009; Wilke and Breuer, 1999). This observation is in support with the reduce band gap found by the Tauc plot, the highest surface area analysis by S_{BET}, and the XRD plane intensity ratio (101/110). The escalation in photocatalytic behaviour of the TiO_2 transition metal was ascribed to narrower crystalline dimension, larger surface area, decreased band gap capacity, lesser electron-hole recombination rate and greater electron-hole generation performance than pure TiO_2 (Liu et al, 2011; Whang et al., 2009). As shown in Fig. 8, Ag-$TiVO_x$ photocatalytic nanocomposites did not show any significant decrease in its activity, after the experiments was repeated three times using the same sample after the first 15 min. This suggest the economy viability of the synthesised photocatalyst.

4. Conclusion

Synthesis of silver, vanadium and silver/vanadium/titanium dioxide (TiO_2, Ag-TiO_2, V-TiO_2 and Ag-$TiVO_x$) nanocomposite photocatalyst by a sol–gel hydrothermal method was achieved. The photocatalytic actions of Ag-$TiVO_x$, relatively to TiO_2, Ag-TiO_2, and V-TiO_2 nanocomposite for MB degradation under visible light irradiation was substantially enhanced. Cantered on the evaluation, a predominantly anatase crystalline phase was achieved. The effect of silver and vanadium showed variation in the band gap contraction. The shift observed as an effect of Ag and V-doped, showed a shift in spectrum to the visible light region. This behaviour resulted in enhance photocatalytic behaviour of the catalyst. All result obtained are evident that doping TiO_2 with Ag, V had attributes in narrowing the band gap, and achieving a well reduced electron-hole recombination. This was due to combining of sensitizing material such as Ag enhancement in the degradation activity of MB supports that a well-defined photocatalyst had been synthesised in the aid to remove pollutant by the means of photocatalytic degradation. This observation of Ag-$TiVO_x$ in comparison with TiO_2, Ag-TiO_2, and V-TiO_2, proves that a more reactive photocatalyst nanocomposite was produced for the removal of organic contaminants. Generally, this study provides an approach for the further enrichment of photocatalytic activities of TiO_2. This strategy might contribute to environmental remediation, using an effective photocatalyst to remove pollutant or contaminants in the environment.

Acknowledgment

Authors will like to appreciate funding of URC of University of Johannesburg. Prof T. C. Jen would like to acknowledge the financial support from NRF of South Africa as well.

References

Bourezgui, A., Kacem, I., Daoudi, M., Al-Hossainy, A.F., 2020. Influence of gamma-irradiation on structural, optical and photocatalytic performance of TiO_2 nanoparticles under controlled atmospheres. J. Elec. Mater. 49 (3), 1904–1921.

Bouzid, H., Faisal, M., Harraz, F.A., Al-Sayari, S.A., Ismail, A.A., 2015. Synthesis of mesoporous Ag/ZnO nanocrystals with enhanced photocatalytic activity. Catal. Today 252, 20–26 https://doi:10.1016/j.cattod.2014.10.011.

Bumajdad, A., Madkour, M., 2014. Understanding the superior photocatalytic activity of noble metals modified titania under UV and visible light irradiation. PCCP 16 (16), 7146–7158. https://doi.org/10.1039/c3cp54411g.

Chen, W.-F., Koshy, P., Adler, L., Sorrell, C.C., 2017. Photocatalytic activity of V-doped TiO_2 thin films for the degradation of methylene blue and rhodamine B dye solutions. J. Aust. Ceram. Soc. 53 (2), 569–576.

Choi, J., Park, H., Hoffmann, M.R., 2010. Effects of single metal-ion doping on the visible-light photoreactivity of TiO 2. J. Phys. Chem. C 114 (2), 783–792.

Díaz-Uribe, C., Viloria, J., Cervantes, L., Vallejo, W., Navarro, K., Romero, E., Quiñones, C., 2018. Photocatalytic activity of Ag-TiO 2 composites deposited by photoreduction under UV irradiation. Int. J. Photoenergy 2018, 1–8.

Dolgonos, A., Mason, T.O., Poeppelmeier, K.R., 2016. Direct optical band gap measurement in polycrystalline semiconductors: A critical look at the Tauc method. J. Solid State Chem. 240, 43–48.

Faisal, M., Ismail, A.A., Harraz, F.A., Al-Sayari, S.A., El-Toni, A.M., Al-Assiri, M.S., 2016. Synthesis of highly dispersed silver doped g-C 3 N 4 nanocomposites with enhanced visible-light photocatalytic activity. Mater. Des. 98, 223–230 https://doi:10.1016/j.matdes.2016.03.019.

Gázquez, M.J., Bolívar, J.P., Garcia-Tenorio, R., Vaca, F., 2014. A review of the production cycle of titanium dioxide pigment. MSA 05 (07), 441–458.

Hwang, S.H., Kim, C., Jang, J., 2011. SnO_2 nanoparticle embedded TiO_2 nanofibers — Highly efficient photocatalyst for the degradation of rhodamine B. Catal. Commun. 12 (11), 1037–1041.

Le, H.A., Linh, L.T., Chin, S., Jurng, J., 2012. Photocatalytic degradation of methylene blue by a combination of TiO2-anatase and coconut shell activated carbon. Powder Technol. 225, 167–175 https://doi:10.1016/j.powtec.2012.04.004.

Li, C., Zhu, N., Dong, X., Zhang, X., Chen, T., Zheng, S., Sun, Z., 2020. Tuning and controlling photocatalytic performance of TiO_2/kaolinite composite towards ciprofloxacin: Role of 0D/2D structural assembly. Adv. Powder Technol. 31 (3), 1241–1252.

Liu, J., Han, R., Zhao, Y., Wang, H., Lu, W., Yu, T., Zhang, Y., 2011. Enhanced photoactivity of V–N Codoped TiO_2 derived from a two-step hydrothermal procedure for the degradation of PCP–Na under visible light irradiation. J. Phys. Chem. C 115 (11), 4507–4515.

Liu, G., Qin, J., Zhou, Z., Liu, C., Li, F., Wu, W., 2019. Mesoporous V-TiO 2 catalysts with crystalline anatase-rutile mixed phases for naphthalene degradation. Chem. Select 4 (44), 12955–12962.

Imoisili, P.E., Dagogo, I.T., Popoola, A.V., Okoronkwo, A.E., 2018. Effect of microwave radiation on the macromolecular, morphological and crystallographic structures of plantain (Musa paradisiaca) Fibre. J. Mater. Environ. Sci. 9 (4), 1301–1305 https://doi.org/10.26872/jmes.2018.9.4.141.

Ismail, A.A., 2012. Facile synthesis of mesoporous Ag-loaded TiO_2 thin film and its photocatalytic properties. Microporous Mesoporous Mater. 149 (1), 69–75.

Ismail, A.A., Matsunaga, H., 2007. Influence of vanadia content onto TiO_2–SiO_2 matrix for photocatalytic oxidation of trichloroethylene. Chem. Phys. Lett. 447 (1–3), 74–78 https://doi:10.1016/j.cplett.2007.08.075.

Pawar, M., Topcu Sendoğdular, S., Gouma, P., 2018. A brief overview of TiO_2 photocatalyst for organic dye remediation: Case study of reaction mechanisms involved in Ce-TiO_2 Photocatalysts System. J. Nanomater. 2018, 1–13.

Rahimi, N., Pax, R.A., Gray, E.M., 2016. Review of functional titanium oxides. I: TiO_2 and its modifications. Prog. Solid State Chem. 44 (3), 86–105.

Reddy, B.M., Chaudhary, B., Ganesh, I., Rojas, T.C., 1998. Characterization of V_2O_5/TiO_2–ZrO_2 catalyst by XPS and other techniques. J. Phys. Chem. B 102 (50), 10176–10182. https://doi.org/10.1021/jp9826165.

Ren, J., Wang, W., Sun, S., Zhang, L., Chang, J., 2009. Enhanced photocatalytic activity of Bi_2WO_6 loaded with Ag nanoparticles under visible light irradiation. Appl. Catal. B 92 (1-2), 50–55.

Ruffino, F., Crupi, I., Simone, F., Grimaldi, M.G., 2011. Formation and evolution of self-organized Au nanorings on indium-tin-oxide surface. Appl. Phys. Lett. 98 (2), 023101. https://doi.org/10.1063/1.3536526.

Sangpour, P., Hashemi, F., Moshfegh, A.Z., 2010. Photoenhanced degradation of methylene blue on cosputtered M:TiO_2 (M = Au, Ag, Cu) nanocomposite systems: A comparative study. J. Phys. Chem. C 114 (33), 13955–13961.

Sanzone, G., Zimbone, M., Cacciato, G., Ruffino, F., Carles, R., Privitera, V., Grimaldi, M.G., 2018. Ag/TiO_2 nanocomposite for visible light-driven photocatalysis. Superlattices Microstruct. 123, 394–402.

Schneider, J., Matsuoka, M., Takeuchi, M., Zhang, J., Horiuchi, Y.u., Anpo, M., Bahnemann, D.W., 2014. Understanding TiO_2 photocatalysis: Mechanisms and materials. Chem. Rev. 114 (19), 9919–9986.

Shao, G.N., Imran, S.M., Jeon, S.J., Kang, S.J., Haider, S.M., Kim, H.T., 2015. Sol–gel synthesis of vanadium doped titania: Effect of the synthetic routes and investigation of their photocatalytic properties in the presence of natural sunlight. Appl. Surf. Sci. 351, 1213–1223.

Shi, W., Duan, D., Wang, H., Ma, C., Sun, Z., Song, X., 2019. Improving the photocatalytic performance of a sea-cucumber-like nanoporous TiO_2 loaded with Pt, Ag for water splitting. Int. J. Hydrogen Energy 44 (26), 13040–13051.

Tripathi, A.M., Nair, R.G., Samdarshi, S.K., 2010. Visible active silver sensitized vanadium titanium mixed metal oxide photocatalyst nanoparticles through sol–gel technique. Sol. Energy Mater. Sol. Cells 94 (12), 2379–2385.

Weng, K.-W., Han, S., 2017. Photocatalytic performance of $TiVO_x$ /TiO_2 thin films prepared by bipolar pulsed magnetron sputter deposition. J. Vacuum Sci. Technol. B, Nanotechnol. Microelectr. Mater. Process. Measure. Phenomena 35 (4), 041207. https://doi.org/10.1116/1.4993435.

Whang T., Huang H., Hsieh M. and Chen, J., 2009. Laser-Induced Silver Nanoparticles on Titanium Oxide for Photocatalytic Degradation of Methylene Blue. Int. J. Mol. Sci. 10, 4707-4718. https://doi.org/10.3390/ijms10114707

Wilke, K., Breuer, H.D., 1999. The influence of transition metal doping on the physical and photocatalytic properties of titania. J. Photochem. Photobiol., A 121 (1), 49–53.

Wu, R.-J., Chen, C.-C., Lu, C.-S., Hsu, P.-Y., Chen, M.-H., 2010. Phorate degradation by TiO_2 photocatalysis: Parameter and reaction pathway investigations. Desalination 250 (3), 869–875 https://doi:10.1016/j.desal.2009.03.026.

Yang, X., Ma, F., Li, K., Guo, Y., Hu, J., Li, W., Huo, M., Guo, Y., 2010. Mixed phase titania nanocomposite codoped with metallic silver and vanadium oxide: New efficient photocatalyst for dye degradation. J. Hazard. Mater. 175 (1-3), 429–438.

Zhang, H., Wang, G., Chen, D.a., Lv, X., Li, J., 2008. Tuning photoelectrochemical performances of Ag−TiO_2 nanocomposites via reduction/oxidation of Ag. Chem. Mater. 20 (20), 6543–6549.

Zhu, X.-D., Zheng, Y.-L., Feng, Y.-J., Sun, K.-N., 2018. Delicate Ag/V_2O_5/TiO_2 ternary nanostructures as a high-performance photocatalyst. J. Solid State Chem. 258, 691–694.